Extensive Pacific deep water expansion contributed to the last glacial atmospheric CO_2 decline

J. Yu[1,2]*, L. Menviel[3], Z.D. Jin[4,5], R.F. Anderson[6], Z. Jian[7], A.M. Piotrowski[8], X. Ma[2], E.J. Rohling[1,9], F. Zhang[2,4], G. Marino[1,10], Jerry McManus[6]

[1]Research School of Earth Sciences, The Australian National University, Canberra, ACT 2601, Australia.
[2]State Key Laboratory of Loess and Quaternary Geology, Institute of Earth Environment, Chinese Academy of Sciences, Xi'an 710075, China.
[3]Climate Change Research Centre, University of New South Wales, Sydney, NSW 2052, Australia.
[4]CAS Center for Excellence in Quaternary Science and Global Change, Xi'an, 710061, China.
[5]Open Studio for Oceanic-Continental Climate and Environment Changes, Qingdao National Laboratory for Marine Science and Technology, Qingdao, 266061, China.
[6]Lamont-Doherty Earth Observatory, Columbia University, New York, New York, 10964, USA.
[7]State Key Laboratory of Marine Geology, Tongji University, Shanghai, 200092, China.
[8]Department of Earth Sciences, University of Cambridge, Cambridge, CB2 3EQ, UK.
[9]Ocean and Earth Science, University of Southampton, National Oceanography Centre, Southampton SO14 3ZH, UK.
[10]Department of Marine Geosciences and Territorial Planning, University of Vigo, 36310 Vigo, Spain.

*Correspondence to: jimin.yu@anu.edu.au

Revised for *Nature Geoscience* as an Article

Although critical for global climate and the carbon cycle, the nature of past ocean circulation changes remains elusive. Based on deep-water carbonate ion ($[CO_3^{2-}]$) reconstructions for wide locations, we discover a low-$[CO_3^{2-}]$ water mass in the South Atlantic at ~3-4 km (extending northward up to ~20°S) during the Last Glacial Maximum. Multiple proxies suggest that this low-$[CO_3^{2-}]$ signal likely reflects an extensive expansion of carbon-rich Pacific deep waters, revealing an ocean circulation scheme different from the long-held view for the glacial deep Atlantic. Comparison of high-resolution $[CO_3^{2-}]$ records from different water depths in the South Atlantic indicates that this expansion occurred between ~38 and ~28 thousand years ago. We infer that the associated carbon sequestration might have contributed critically to the contemporary ~20 ppm atmospheric CO_2 decline and thereby helped pushing the global climate to the glacial maximum.

Ocean circulation and the carbon cycle are intricately linked, and ocean circulation reconstructions can therefore provide important insights into mechanisms for past atmospheric CO_2 changes. Ocean circulation in the deep Atlantic Ocean (>~2.5 km) during the Last Glacial Maximum (LGM; 18-22 ka) is traditionally viewed to follow a mixing model between northern- and southern-sourced deep waters produced in the polar Atlantic, without much need to involve waters from other oceans[1-4]. Using this long-held ocean circulation model, however, it is difficult to explain the observed older radiocarbon ages (^{14}C ages) and more radiogenic neodymium isotopic (εNd) signatures at ~3.8 km than at ~5 km in the LGM South Atlantic[5,6] (Fig. 1). Burke et al.[7] showed that sluggish recirculation of southern-sourced waters combined with reduced mixing with ^{14}C-rich northern-sourced waters can contribute to the old ^{14}C ages at ~3.8 km, in the

absence of interocean water-mass interactions. Nevertheless, additional mechanisms are likely necessary to fully explain the depth structure and large magnitude of ^{14}C-age changes as well as the more radiogenic εNd signal observed at the same depth (Fig. 1). Robinson and Van de Flierdt[8] suggested that changes in Pacific deep waters (PDW) can significantly affect deglacial εNd signatures in the Drake Passage (Southern Ocean), but their role in the deep South Atlantic during the LGM remains unexplored. PDW stores a large amount of respired carbon[9,10], and thus its changes including volumetric extension and associated timing would have important implications for past atmospheric CO_2 variations.

Deep water carbonate ion concentrations ($[CO_3^{2-}]$) have great potential to provide critical information about past deep ocean circulation and dissolved inorganic carbon (DIC) changes. In the modern Atlantic, contrasting $[CO_3^{2-}]$ signatures between water masses highlight ocean circulation patterns[11] (Fig. 2). Also, past DIC changes may be quantified from $[CO_3^{2-}]$ reconstructions[12]. Here, we present deep-water $[CO_3^{2-}]$ reconstructions for extensive locations in the Atlantic to decipher the role of ocean circulation in the glacial atmospheric CO_2 decrease. We focus on the deep South Atlantic hydrography, an intensively studied but yet not fully understood subject in palaeoceanography[5-8,13-16].

First meridional $[CO_3^{2-}]$ transect for the LGM deep Atlantic

We have reconstructed deep-water $[CO_3^{2-}]$ using benthic B/Ca for the Holocene (0-5 ka) and LGM samples from 41 cores (Fig. 2; Supplementary Fig. 1-3). To address radiocarbon and εNd anomalies at 3.8 km water depth as illustrated in Fig. 1, five cores at 3-4.2 km and an abyssal core (TNO57-21) at ~5 km from the South Atlantic were chosen for investigation (Fig. 2a). Thirty

additional cores from widely spread locations (1.1-4.7 km, 36°S-62°N) in the Atlantic and 5 cores at 3-4 km from the equatorial Pacific are used to provide a broader context of water mass signatures. Benthic B/Ca is converted into deep-water [CO_3^{2-}] using species-specific sensitivities based on global core-top calibrations[17]. The uncertainty associated with [CO_3^{2-}] reconstructions is ~5 μmol/kg[17]. Detailed information about samples and analytical methods along with new (n = 173 samples) and compiled (n = 260 samples) data used is given in Methods and Supplementary Tables 1-11.

Fig. 2c shows the first meridional [CO_3^{2-}] transect for the deep Atlantic during the LGM (Methods). Given the locations of studied cores, this transect should be deemed to mainly reflect [CO_3^{2-}] distributions for the eastern Atlantic basins. Future work is needed to investigate any zonal homogeneity in the LGM Atlantic. Nevertheless, the features revealed by Fig. 2c can be used to infer ocean circulation changes at the LGM. Compared with the modern distribution, [CO_3^{2-}] of glacial North Atlantic waters above ~2.5 km reached up to ~140 μmol/kg, which is ~20 μmol/kg higher than that of North Atlantic Deep Water (NADW)[11]. These waters likely represent previously documented well-ventilated Glacial North Atlantic Intermediate Waters (GNAIW)[1,2,18,19]. Below ~2.5 km, LGM North Atlantic [CO_3^{2-}] values were up to ~20 μmol/kg lower than today, consistent with greater mixing/advection of low-[CO_3^{2-}] Glacial Antarctic Bottom Waters (GAABW) and/or increased respiration in the glacial ocean[1,2,19,20]. The boundary of ~2.5 km delineated by LGM upper and lower water masses is consistent with that found from other proxies ($\delta^{13}C$, Cd/Ca, and εNd) and model results[1-3,19,21,22].

In the South Atlantic, deep-water [CO_3^{2-}] in the 5 studied cores from ~3-4 km water depth are lower by ~20 μmol/kg during the LGM than the Holocene, consistent with qualitative [CO_3^{2-}] proxies from the same cores[23-25] (Supplementary Fig. 2). By contrast, opposite LGM-Holocene [CO_3^{2-}] changes are observed in the abyssal core TNO57-21 (41.1°S, 7.8°E, 4981 m). TNO57-21 shows slightly higher deep-water [CO_3^{2-}] values during the LGM than the Holocene, supported by multiple benthic B/Ca measurements in this core and qualitative proxies including %$CaCO_3$ and foraminiferal fragmentation data for several South Atlantic cores at similar water depths[15,23,24] (Supplementary Fig. 3). Our data reveal a low-[CO_3^{2-}] (<80 μmol/kg) water mass centered at ~3.5 km and extending northward up to ~20°S, which overlay a relatively high-[CO_3^{2-}] (>80 μmol/kg) water mass at abyssal depth in the LGM South Atlantic.

Ocean circulation and biological influences within the Atlantic

Below, we discuss the nature of our newly discovered low-[CO_3^{2-}] deep South Atlantic water mass (Fig. 2). Deep-water [CO_3^{2-}] is affected by changes in endmember values, biogenic matter respiration, and water mass mixing. We combine [CO_3^{2-}] with benthic $\delta^{13}C$ and εNd to investigate influences from these processes (Fig. 3). To provide a context, we start with the Holocene data. Modern water mass endmember values are assigned following the literature[1,3,26]. As can be seen from Fig. 3a and b, Holocene deep-water signatures at studied cores, including the 5 cores at ~3-4 km from the South Atlantic, fall along the NADW-AABW mixing trends, consistent with the established knowledge[1-3,19].

For the LGM, we first investigate water mass endmember changes (Fig. 3c, d). To do so, we identify sites with benthic $\delta^{13}C$ values similar to the $\delta^{13}C$ endmembers as defined by ref. [1-3,19].

Deep-water [CO_3^{2-}] reconstructions for the same sites are chosen as corresponding [CO_3^{2-}] end-members of water masses. Thus, we choose $\delta^{13}C$ = ~1.5‰ and [CO_3^{2-}] = ~140 μmol/kg as endmember values for GNAIW, and $\delta^{13}C$ = ~-0.8‰ and [CO_3^{2-}] = ~85 μmol/kg for GAABW (Supplementary Table 3). The εNd endmember for GNAIW is debated[3,27], and we assign a range of values of ~-13.5 to ~-10.5 to this water mass. Using other εNd values for GNAIW would have little influence on our conclusions, as long as GNAIW had a less radiogenic εNd than GAABW. For GAABW, we choose LGM εNd measurements (~-6.7) from TNO57-21[6], the same site used to pin down $\delta^{13}C$ and [CO_3^{2-}] endmember values[1]. Our choice is different from ref. [3] which used LGM measurements for MD07-3076Q as GAABW εNd. Compared to TNO57-21 (5 km), MD07-3076Q (44.2°S, 14.2°W, 3770 m) is located at a much shallower water depth (3.8 km) near the mid ocean ridge, and was bathed in warmer and less saline deep waters during the LGM[28]. By contrast, core TNO57-21 was retrieved from the abyssal Cape Basin, and is ideally located downstream of AABW formed on Antarctic shelves. Previous pore water reconstructions suggest extremely cold and saline waters in the abyssal Cape Basin during the LGM[16], lending strong support to using TNO57-21 for determining GAABW endmember values.

Given the above endmember values, it is impossible to explain the low-[CO_3^{2-}] water mass signature at ~3-4 km in the LGM South Atlantic by conservative mixing between GNAIW and GAABW because this water had even lower [CO_3^{2-}] values than GAABW (Fig. 2, 3). Previous work[7,29,30] suggested possible sluggish recirculation of GAABW in the lower cell (>~2.5 km) of the Atlantic during the LGM. In this case, one might view the South Atlantic low-[CO_3^{2-}] signature at ~3-4 km as a consequence of accumulation of respired carbon due to water mass aging, analogous to the cause of the low-[CO_3^{2-}] signature of PDW in the modern ocean[11,31]

(Supplementary Fig. 4). Any respiration would decrease $\delta^{13}C$ and $[CO_3^{2-}]$ along the Redfield slope, with little impact on εNd[3,26]. Were the low-$[CO_3^{2-}]$ in the five South Atlantic cores indeed due to enhanced respiration effects, then the combined $[CO_3^{2-}]$ and $\delta^{13}C$ values would imply an almost pure GNAIW source water (Fig. 3c). However, this would contradict with much more radiogenic εNd values (-5 to -9) than those of GNAIW (~-13.5 to ~-10.5) (Fig. 3d). We therefore conclude that the low-$[CO_3^{2-}]$ signature of the LGM South Atlantic water mass at 3-4 km cannot be simply explained by a combination of mixing and respiration of GNAIW and GAABW endmembers.

Expansion of glacial Pacific deep waters into the South Atlantic

Considering that deep waters from the Pacific generally have high-DIC and low-$[CO_3^{2-}]$ values[11,18], we explore whether the low-$[CO_3^{2-}]$ water mass recorded by the 5 South Atlantic cores was affected by Glacial Pacific Deep Waters (GPDW). The GPDW endmember $\delta^{13}C$ and εNd values are assigned to be -0.4‰ and -3.5, respectively, based on the published data[32-34] (Fig. 3; Supplementary Table 3). Currently, there is no benthic B/Ca data to define the GPDW $[CO_3^{2-}]$ endmember due to intensive dissolution and rare abundance of required mono-species in the deep North Pacific. Nevertheless, foraminiferal assemblage and boron isotope (based on mixed *Cibicides*) data[35,36] suggest similar $[CO_3^{2-}]$ values between the Holocene and the LGM in this region. Therefore, we assume GPDW had the same endmember $[CO_3^{2-}]$ value (~50 μmol/kg) as PDW. We acknowledge potential uncertainties with this endmember. However, to draw our main conclusion, what is required is a lower $[CO_3^{2-}]$ for GPDW than for GAABW, which is supported by published data[18,37,38]. Located downstream of GPDW, all examined cores at 3-4 km from the equatorial Pacific show lower LGM $[CO_3^{2-}]$ (61-76 μmol/kg) than GAABW (>80 μmol/kg) (Fig. 3c). In the modern ocean, PDW $[CO_3^{2-}]$ increases during its southward transport due to mixing

with younger and lower-DIC waters (Supplementary Fig. 3). Benthic $\delta^{13}C$ mapping[32] indicates that the basic ocean circulation pattern seen today operated in the LGM Pacific. Therefore, GPDW likely had a lower [CO_3^{2-}] than GAABW, a situation also expected from much older age and likely more respired carbon associated with GPDW[36,39].

In the [CO_3^{2-}]-$\delta^{13}C$ space, data from the five South Atlantic cores suggest a mixing scheme involving three water masses: GNAIW, GAABW, and GPDW (Fig. 3c). This mixing scheme can also explain low [CO_3^{2-}] and more radiogenic εNd values at these locations by mixing GPDW with aged GNAIW-GAABW mixtures (Fig. 3d), although insufficient knowledge of endmember εNd and Nd contents preclude exact mixing scenarios and respiration effects (Supplementary Fig. 5, 6). Paired [CO_3^{2-}]-^{14}C age data are too limited to allow a detailed investigation, but mixing of GPDW into the LGM South Atlantic is qualitatively consistent with the very old ventilation age at MD07-3076Q (Fig. 1)[5]. Therefore, we attribute the low [CO_3^{2-}] values at 3-4 km in the LGM South Atlantic to admixture of low-[CO_3^{2-}] GPDW. The low-[CO_3^{2-}] deep-water occupation to ~20°S in the South Atlantic suggests substantial expansion of GPDW during the LGM (Fig. 2c). This is different from the long-held view which largely focuses on changes in water masses formed in the glacial Atlantic.

Prevailing evidence suggests a sluggish circulation, characterized by reduced water mass mixing in the LGM Pacific Ocean[21,22,32]. This would allow southward expansion of the recirculated GPDW to better preserve its low-[CO_3^{2-}], more-radiogenic-εNd, and old-^{14}C age signatures during transport. This is indeed supported by findings of a "floating" high-DIC, low-[CO_3^{2-}], and very old water mass in the equatorial and South Pacific during the LGM[18,40]. Entrainment into the Antarctic

Circumpolar Current at the latitude of Drake Passage (~60°S) would have facilitated GPDW transport into the South Atlantic[31], analogues to what happens today but with greater influences from GPDW in the LGM Southern Ocean (Supplementary Fig. 7). In contrast to vigorous and deep southward NADW transport today, shoaled GNAIW formation would allow greater northward expansion of GPDW in the deep (>~2.5 km) Atlantic at the LGM (Fig. 2). Nevertheless, owing to inevitable mixing with surrounding waters during transport, we use modified GPDW (mGPDW) in Fig. 2c to indicate its remote source from the LGM North Pacific.

It's worth noting that our proposed GPDW expansion does not necessarily exclude recirculation within the LGM Atlantic as suggested previously[7]. Instead, it is likely that both processes are needed to fully explain proxy data in the LGM ocean. We also note that GAABW $\delta^{13}C$ is a matter of long-lasting debate[41], but consideration of other scenarios to define this endmember does not affect our conclusion (Supplementary Fig. 8).

Timing of GPDW expansion and implications for atmospheric CO_2

To determine the timing of GPDW expansion, we have extended the previously published $[CO_3^{2-}]$ record (0-27 ka)[42] to 60 ka for core TNO57-21 (downstream of GAABW), and then compare it with a previously published $[CO_3^{2-}]$ record from core MD07-3076Q[25] which is located close to the core of the low-$[CO_3^{2-}]$ water mass (Fig. 2, 4). Before ~38 ka, the long-term deep-water $[CO_3^{2-}]$ at 3.8 km (MD07-3076Q) was slightly higher than at 5 km (TNO57-21), similar to the preindustrial bathymetric $[CO_3^{2-}]$ distribution in the South Atlantic[11] (Fig. 2a). From ~38 to ~28 ka, the vertical $[CO_3^{2-}]$ gradient reversed between the two depths, coeval with a significant ageing of deep waters at MD07-3076Q[43]. This reversal broadly corresponded to the maximum

advance of the Antarctic ice sheet, possibly associated with a weakening of GAABW[21,22]. If so, reduced GAABW production might have facilitated the development of the low-[CO_3^{2-}] anomaly at 3-4 km in the South Atlantic. By ~20 ka, deep-water [CO_3^{2-}] at 3.8 km was ~15 μmol/kg lower than at 5 km, suggesting full establishment of low-[CO_3^{2-}] GPDW expansion in the South Atlantic (Fig. 2). Superimposed on the long-term changes, we find that deep-water [CO_3^{2-}] converged between MD07-3076 and TNO57-21 during Heinrich Stadials, consistent with previously reconstructed erosion of chemical gradients in the deep Southern Ocean due to enhanced vertical mixing[43,44]. Therefore, the large and reversed [CO_3^{2-}] gradient between MD07-3076Q and TNO57-21 lends strong support to the role of sluggish ocean circulation in sequestering carbon during the LGM[21,22].

Our deep-water [CO_3^{2-}] reconstructions offer a means to quantify carbon storage changes in the past. Below 3 km water depth, Atlantic [CO_3^{2-}] was ~15 μmol/kg lower on average during the LGM relative to preindustrial times (Fig. 2; Supplementary Table 4). Based on the relationship from ref. [12], this suggests at least ~25 μmol/kg increase in DIC. Using a mass of 10×10^{19} kg for waters below 3 km in the Atlantic, this implies that the deep Atlantic sequestered ~30 Gigatonnes extra carbon during the LGM relative to the preindustrial. But, this estimate likely represents a lower limit of carbon sequestration. If our inferred GPDW expansion is correct, then it would imply extensive occupation of low-[CO_3^{2-}] and high-DIC deep waters in the voluminous Indo-Pacific oceans. Respired carbon contents are high in the deep Pacific today, and may have been even higher during the LGM, as suggested by reduced glacial deep-sea O_2 levels[9,10]. By increasing sequestration of respired carbon and nutrient in the ocean interior, GPDW expansion would decrease the preformed nutrient levels[10], enhance the global biological pump efficiency, and thus

lower atmospheric CO_2. Given coeval low-[CO_3^{2-}] water mass formation and the ~20 ppm atmospheric CO_2 drop[45] (Fig. 4), we suggest that expansion of high-DIC GPDW into the deep South Atlantic was a key contributor to the final atmospheric CO_2 drawdown and thereby helped pushing the global climate to the glacial maximum.

Methods

Samples and analytical methods. For the LGM Atlantic transect mapping (Fig. 2), we have measured (n = 19 cores) and compiled (n = 22 cores) benthic B/Ca for 41 sediment cores from the Atlantic and Pacific oceans. Age models are based on published chronologies (see Supplementary Table 1). For three cores, samples from <~8 ka are treated as the Holocene age (defined as 0-5 ka here), but exclusion of these samples do not affect our conclusion. For new samples analyzed in this study, sediments (~10-20 cm^3 from ~2 cm thickness each) were disaggregated in de-ionized water and wet sieved through 63 μm sieves. Except for ODP 1087 for which *C. mundulus* was used, we picked *C. wuellerstorfi* (generally ~10-20 tests for each sample) from the 250-500 μm size fraction. The shells were double checked under a microscope before crushing to ensure consistent shell morphology used for measurements. Following this careful screening the starting material for each sample was on average ~8-12 shells, which is equivalent to ~300-600 μg of carbonate. For benthic B/Ca analyses, foraminiferal shells were cleaned with the "Mg-cleaning" method[46]. Benthic B/Ca ratios were measured on an inductively-coupled plasma mass spectrometer (ICP-MS) using procedures outlined in ref. [47], with an analytical error better than ~5%. Regarding down-core analyses for TNO57-21, we have extended the benthic

B/Ca record back to 60 ka, following the same approach given in ref. [42]. We have also measured benthic stable isotopes for 4 cores, with analytical precision of ~0.08‰ for $\delta^{18}O$ and $\delta^{13}C$.

All new (n = 173 samples) and compiled (n = 260 samples) [CO_3^{2-}] reconstructions together with paired benthic $\delta^{13}C$ and εNd are provided in the Supplementary Tables 1-11.

Deep water [CO_3^{2-}] reconstructions. Deep-water [CO_3^{2-}] values are reconstructed using benthic B/Ca[12,17] from $[CO_3^{2-}]_{downcore} = [CO_3^{2-}]_{PI} + \Delta B/Ca_{downcore-coretop}/k$, where $[CO_3^{2-}]_{PI}$ is the preindustrial (PI) deep-water [CO_3^{2-}] value estimated from the GLODAP dataset[11], $\Delta B/Ca_{downcore-coretop}$ represents the deviation of B/Ca of down-core samples from the core-top value, and k is the B/Ca-[CO_3^{2-}] sensitivity of *C. wuellerstorfi* (1.14 μmol/mol per μmol/kg) or *C. mundulus* (0.69 μmol/mol per μmol/kg)[17]. To calculate [CO_3^{2-}], we have removed anthropogenic influences on DIC after ref. [48]. We use a reconstruction uncertainty of 5 μmol/kg (1σ) in [CO_3^{2-}] based on global core-top calibration samples[17].

Mapping of LGM [CO_3^{2-}] data. Given limited number reconstructions as almost always the case for palaeo, all cores are projects onto a single, arbitrary latitudinal-water depth plane for the LGM plotting (Fig. 2c), an approach widely used for mapping of other proxies like εNd and $\delta^{13}C$[1,3,19]. Ocean Data View is employed to generate Fig. 2c using the average [CO_3^{2-}] values (Supplementary Table 2).Contours are generated using the DIVA gridding with X and Y scale-length values of 110 and 104, respectively. Quality limit is set to 7. Linear mapping option is used for color mapping.

Modern seawater [CO_3^{2-}]-$\delta^{13}C$-εNd data. In Fig. 3a, modern seawater [CO_3^{2-}]-$\delta^{13}C$ data are from the GLODAP dataset[11]. εNd data shown in Fig. 3b are compiled from the literature for seawater samples from > 1 km, while their corresponding seawater [CO_3^{2-}] are estimated using the GLODAP dataset[11], not measured along with εNd analyses. Associated data are provided in Supplementary Tables 9-10.

Water mass mixing. The chemical and isotopic signatures of mixtures of two waters are calculated by

$$[X]_M = [X]_A \times f_A + [X]_B \times (1 - f_A) \quad (1)$$

$$\delta_M \times [X]_M = \delta_A \times [X]_A \times f_A + \delta_B \times [X]_B \times (1 - f_A) \quad (2)$$

where [X] and δ are, respectively, endmember concentrations and chemical signatures of tracers (elements or compounds) of interest, subscripts A, B, and M represent water mass A, B and their mixture, respectively, and f_A is the fraction of water mass A in the mixture. Here, X denotes C, Nd, or DIC, while δ represents $\delta^{13}C$, εNd, or [CO_3^{2-}]. Thus, we can obtain

$$\delta_M = (\delta_A \times [X]_A \times f_A + \delta_B \times [X]_B \times (1 - f_A)) \div ([X]_A \times f_A + [X]_B \times (1 - f_A)) \quad (3)$$

The endmember values used to calculate "reference" mixing curves shown in Fig. 3 are given in Supplementary Table 3. The endmember [Nd] values are assumed to be unchanged between modern water masses and their LGM counterparts, but it is important to note that past seawater [Nd] remains poorly constrained.

For the hypothetical aged GNAIW-GAABW mixture shown in Fig. 3d, we use [Nd] = 22 pmol/kg, εNd = -10, $[CO_3^{2-}]$ = 90 μmol/kg, and DIC = 2300 μmol/kg. More scenarios to explain the LGM εNd-$[CO_3^{2-}]$ data are given in Supplementary Fig. 5.

The mixing curvature depends on the relative difference between $[X]_A$ and $[X]_B$. For the $\delta^{13}C$-$[CO_3^{2-}]$ system, the mixing curvature is insensitive to endmember DIC changes because water-mass DIC contrasts are small (<10%) and DIC-weighing applies to both $[CO_3^{2-}]$ and $\delta^{13}C$. By contrast, the curvature is greater for the εNd-$[CO_3^{2-}]$ system, driven by the large [Nd] difference (up to ~50%-100%) between water masses (Fig. 3). A various sensitivity test is given in Supplementary Fig. 6, by changing endmember [Nd] and DIC values.

Note that we assume tracers remain conservative, with no addition or removal of ingredients, during mixing of water masses. This is likely an oversimplification. Thus, mixing lines shown (Fig. 3; Supplementary Fig. 5) should be treated as a guide to aid interpretation of data instead of using them for accurate quantification of mixing ratios. Importantly, insufficient knowledge about [Nd] and the potentially large endmember εNd range for GNAIW (Fig. 3) preclude estimates of exact mixing scenarios for the LGM, although the data do provide useful clues about mixing schemes in a qualitative sense.

Statistical analyses. For TNO57-21 downcore record, uncertainties associated with $[CO_3^{2-}]$ were evaluated using a Monte-Carlo approach[49]. Errors associated with the chronology (x-axis) and $[CO_3^{2-}]$ reconstructions (y-axis) are considered during error propagation. Age errors are estimated following ref. [24]. Error for each $[CO_3^{2-}]$ reconstruction is 5 μmol/kg. All data points were

sampled separately and randomly 5,000 times within their chronological and [CO_3^{2-}] uncertainties and each iteration was then interpolated linearly. At each time step, the probability maximum and data distribution uncertainties of the 5,000 iterations were assessed. Fig. 4a shows ±1σ (dark red envelopes; 16^{th}-84^{th} percentile) and ±2σ (light red; 2.5^{th}-97.5^{th} percentile) probability intervals for the data distributions, including chronological and proxy uncertainties.

References

1. Oppo D, Gebbie G, Huang KF, Curry W, Marchitto T, Pietro KR. Data Constraints on Glacial Atlantic Water Mass Geometry and Properties. *Paleoceanography and Paleoclimatology* 2018, **33**(9)**:** 1013-1034.

2. Lynch-Stieglitz J, Adkins JF, Curry WB, Dokken T, Hall IR, Herguera JC, *et al.* Atlantic meridional overturning circulation during the Last Glacial Maximum. *Science* 2007, **316**(5821)**:** 66-69.

3. Howe JNW, Piotrowski A, Noble TL, Mulitza S, Chiessi CM, Bayon G. North Atlantic Deep Water Production during the Last Glacial Maximum. *Nat Commun* 2016, **7:** doi: 10.1038/ncomms11765.

4. Gebbie G. How much did Glacial North AtlanticWater shoal? *Paleoceanogr* 2014, **29**(3)**:** 190-209.

5. Skinner L, Fallon SJ, Waelbroeck C, Michel E, Barker S. Ventilation of the Deep Southern Ocean and Deglacial CO_2 Rise. *Science* 2010, **328:** 1147-1151.

6. Piotrowski A, Galy A, Nicholl JAL, Roberts N, Wilson DJ, Clegg JA, *et al.* Reconstructing deglacial North and South Atlantic deep water sourcing using foraminiferal Nd isotopes. *Earth Planet Sci Lett* 2012, **357-358:** 289-297.

7. Burke A, Stewart AL, Adkins JF, Ferrari R, Jansen MF, Thompson AF. The glacial mid-depth radiocarbon bulge and its implications for the overturning circulation. *Paleoceanogr* 2015, **30**(7)**:** 1021-1039.

8. Robinson LF, van de Flierdt T. Southern Ocean evidence for reduced export of North Atlantic Deep Water during Heinrich event 1. *Geology* 2009, **37:** 195-198.

9. Anderson RF, Sachs JP, Fleisher MQ, Allen KA, Yu J, Koutavas A, *et al.* Deep-sea oxygen depletion and ocean carbon sequestration during the last ice age. *Glob Biogeochem Cycle* 2019, **0**(ja).

10. Jaccard SL, Galbraith ED. Large climate-driven changes of oceanic oxygen concentrations during the last deglaciation. *Nature Geoscience* 2012, **5**(2)**:** 151-156.

11. Key RM, Kozyr A, Sabine CL, Lee K, Wanninkhof R, Bullister JL, *et al.* A global ocean carbon climatology: Results from Global Data Analysis Project (GLODAP). *Glob Biogeochem Cycle* 2004, **18**(4)**:** doi: 10.1029/2004GB002247.

12. Yu J, Menviel L, Jin ZD, Thornalley DJR, Barker S, Marino G, *et al.* Sequestration of carbon in the deep Atlantic during the last glaciation. *Nature Geoscience* 2016, **9**(4)**:** 319-324.

13. Burke A, Robinson LF. The Southern Ocean's role in carbon exchange during the last deglaciation. *Science* 2012, **335:** 557-561. doi:510.1126/science.1208163.

14. Skinner LC, Scrivner AE, Vance D, Barker S, Fallon S, Waelbroeck C. North Atlantic versus Southern Ocean contributions to a deglacial surge in deep ocean ventilation. *Geology* 2013, **41**(6)**:** 667-670.

15. Barker S, Knorr G, Vautravers M, Diz P, Skinner L. Extreme deepening of the Atlantic overturning circulation during deglaciation. *Nature Geoscience* 2010, **3:** 567-571.

16. Adkins JF, McIntyre K, Schrag DP. The salinity, temperature, and $\delta^{18}O$ of the glacial deep ocean. *Science* 2002, **298**(5599)**:** 1769-1773.

17. Yu JM, Elderfield H. Benthic foraminiferal B/Ca ratios reflect deep water carbonate saturation state. *Earth Planet Sci Lett* 2007, **258**(1-2)**:** 73-86, doi: 10.1016/j.epsl.2007.1003.1025.

18. Yu J, Broecker W, Elderfield H, Jin ZD, McManus J, Zhang F. Loss of carbon from the deep sea since the Last Glacial Maximum. *Science* 2010, **330:** 1084-1087, doi: 1010.1126/science.1193221.

19. Marchitto T, Broecker W. Deep water mass geometry in the glacial Atlantic Ocean: A review of constraints from the paleonutrient proxy Cd/Ca. *Geochem Geophys Geosyst* 2006, **7**(12)**:** doi:10.1029/2006GC001323.

20. Chalk TB, Foster GL, Wilson PA. Dynamic storage of glacial CO2 in the Atlantic Ocean revealed by boron [CO32−] and pH records. *Earth Planet Sci Lett* 2019, **510:** 1-11.

21. Menviel L, Yu J, Joos F, Mouchet A, Meissner KJ, England MH. Poorly ventilated deep ocean at the Last Glacial Maximum inferred from carbon isotopes: A data-model comparison study. *Paleoceanogr* 2017, **31:** doi:10.1002/2016PA003024.

22. Muglia J, Skinner L, Schmittner A. Weak overturning circulation and high Southern Ocean nutrient utilization maximized glacial ocean carbon. *Earth Planet Sci Lett* 2018, **496:** 47-56.

23. Hodell DA, Charles CD, Sierro FJ. Late Pleistocene evolution of the ocean's carbonate system. *Earth Planet Sci Lett* 2001, **192**(2)**:** 109-124.

24. Gottschalk J, Hodell DA, Skinner LC, Crowhurst SJ, Jaccard SL, Charles C. Past Carbonate Preservation Events in the Deep Southeast Atlantic Ocean (Cape Basin) and Their Implications for Atlantic Overturning Dynamics and Marine Carbon Cycling. *Paleoceanography and Paleoclimatology* 2018, **33**(6)**:** 643-663.

25. Gottschalk J, Skinner LC, Misra S, Waelbroeck C, Menviel L, Timmermann A. Abrupt changes in the southern extent of North Atlantic Deep Water during Dansgaard-Oeschger events. *Nature Geoscience* 2015, **8**(12)**:** 950-U986.

26. Yu JM, Elderfield H, Piotrowski A. Seawater carbonate ion-$\delta^{13}C$ systematics and application to glacial-interglacial North Atlantic ocean circulation. *Earth Planet Sci Lett* 2008, **271**(1-4)**:** 209-220. doi:210.1016/j.epsl.2008.1004.1010.

27. Zhao N, Oppo DW, Huang K-F, Howe JNW, Blusztajn J, Keigwin LD. Glacial–interglacial Nd isotope variability of North Atlantic Deep Water modulated by North American ice sheet. *Nat Commun* 2019, **10**(1)**:** 5773.

28. Roberts J, Gottschalk J, Skinner LC, Peck VL, Kender S, Elderfield H, *et al.* Evolution of South Atlantic density and chemical stratification across the last deglaciation. *Proceedings of the National Academy of Sciences* 2016, **113**(3)**:** 514-519.

29. Ferrari R, Jansen MF, Adkins JF, Burke A, Stewart AL, Thompson AF. Antarctic sea ice control on ocean circulation in present and glacial climates. *P Natl Acad Sci USA* 2014, **111**(24)**:** 8753-8758.

30. Adkins JF. The role of deep ocean circulation in setting glacial climates. *Paleoceanogr* 2013, **28**(3)**:** 539-561.

31. Talley LD. Closure of the Global Overturning Circulation Through the Indian, Pacific, and Southern Oceans: Schematics and Transports. *Oceanography* 2013, **26**(1)**:** 80-97.

32. Matsumoto K, Oba T, Lynch-Stieglitz J, Yamamoto H. Interior hydrography and circulation of the glacial Pacific Ocean. *Quat Sci Rev* 2002, **21:** 1693-1704.

33. Hu R, Piotrowski AM, Bostock HC, Crowhurst S, Rennie V. Variability of neodymium isotopes associated with planktonic foraminifera in the Pacific Ocean during the Holocene and Last Glacial Maximum. *Earth Planet Sci Lett* 2016, **447:** 130-138.

34. Keigwin LD. North Pacific deep water formation during the latest glaciation. *Nature* 1987, **330**(6146)**:** 362-364.

35. Anderson DM, Archer D. Glacial-interglacial stability of ocean pH inferred from foraminifer dissolution rates. *Nature* 2002, **416**(6876)**:** 70-73.

36. Rae JWB, Sarnthein M, Foster GL, Ridgwell A, Grootes PM, Elliott T. Deep water formation in the North Pacific and deglacial CO_2 rise. *Paleoceanogr* 2014, **29**(6)**:** 645-667.

37. Umling NE, Thunell RC. Mid-depth respired carbon storage and oxygenation of the eastern equatorial Pacific over the last 25,000 years. *Quat Sci Rev* 2018, **189:** 43-56.

38. Doss W, Marchitto TM. Glacial deep ocean sequestration of CO_2 driven by the eastern equatorial Pacific biologic pump. *Earth Planet Sci Lett* 2013, **377:** 43-54.

39. Galbraith ED, Jaccard SL, Pedersen TF, Sigman DM, Haug GH, Cook M, *et al.* Carbon dioxide release from the North Pacific abyss during the last deglaciation. *Nature* 2007, **449:** 890-893.

40. Ronge TA, Tiedemann R, Lamy F, Köhler P, Alloway BV, De Pol-Holz R, *et al.* Radiocarbon constraints on the extent and evolution of the South Pacific glacial carbon pool. *Nat Commun* 2016, **7:** 11487.

41. Gottschalk J, Vázquez Riveiros N, Waelbroeck C, Skinner LC, Michel E, Duplessy J-C, *et al.* Carbon isotope offsets between benthic foraminifer species of the genus Cibicides (Cibicidoides) in the glacial sub-Antarctic Atlantic. *Paleoceanogr* 2016, **31**(12)**:** 1583-1602.

42. Yu J, Anderson RF, Jin ZD, Menviel L, Zhang F, Ryerson FJ, *et al.* Deep South Atlantic carbonate chemistry and increased interocean deep water exchange during last deglaciation. *Quat Sci Rev* 2014.

43. Gottschalk J, Skinner LC, Lippold J, Vogel H, Frank N, Jaccard SL, *et al.* Biological and physical controls in the Southern Ocean on past millennial-scale atmospheric CO2 changes. *Nat Commun* 2016, **7:** 11539.

44. Basak C, Fröllje H, Lamy F, Gersonde R, Benz V, Anderson RF, *et al.* Breakup of last glacial deep stratification in the South Pacific. *Science* 2018, **359**(6378)**:** 900-904.

45. Bereiter B, Eggleston S, Schmitt J, Nehrbass-Ahles C, Stocker TF, Fischer H, *et al.* Revision of the EPICA Dome C CO2 record from 800 to 600 kyr before present. *Geophysical Research Letters* 2015, **42**(2)**:** 542-549.

46. Barker S, Greaves M, Elderfield H. A study of cleaning procedures used for foraminiferal Mg/Ca paleothermometry. *Geochem Geophys Geosyst* 2003, **4**(9)**:** doi:10.1029/2003GC000559.

47. Yu JM, Day J, Greaves M, Elderfield H. Determination of multiple element/calcium ratios in foraminiferal calcite by quadrupole ICP-MS. *Geochem Geophys Geosyst* 2005, **6:** Q08P01, doi:10.1029/2005GC000964.

48. Feely RA, Sabine C, Lee K, Berelson WM, Kleypas J, Fabry VJ, *et al.* Impact of anthropogenic CO_2 on the $CaCO_3$ system in the oceans. *Science* 2004, **305:** 362-366.

49. Grant KM, Rohling EJ, Bar-Matthews M, Ayalon A, Medina-Elizalde M, Bronk Ramsey C, *et al.* Rapid coupling between ice volume and polar temperature over the past 150,000 years. *Nature* 2012, **491:** 744-747.

50. Schlitzer R. Ocean Data View. 2006, **http://odv.awi-bremerhaven.de**.

Acknowledgments: All data accompanying this study are available from PANGAEA (doi.pangaea.de/xxx) and Supplementary Information. This work is supported by ARC Discovery Projects (DP140101393, DP190100894) and Future Fellowship (FT140100993) and NSFC41676026 to JY, DECRA (DE150100107) and Discovery (DP180100048) to LM, and Australian Laureate Fellowship (FL120100050) to EJR.

Author contributions. JY designed the project and wrote the paper with inputs from all authors.

Additional information. Supplementary information is available in the online version of the paper with inputs from all authors. Reprints and permissions information is available online at www.nature.com/reprints. Correspondence and requests for materials should be addressed to J.Y.

Competing interests. The authors declare no competing interests.

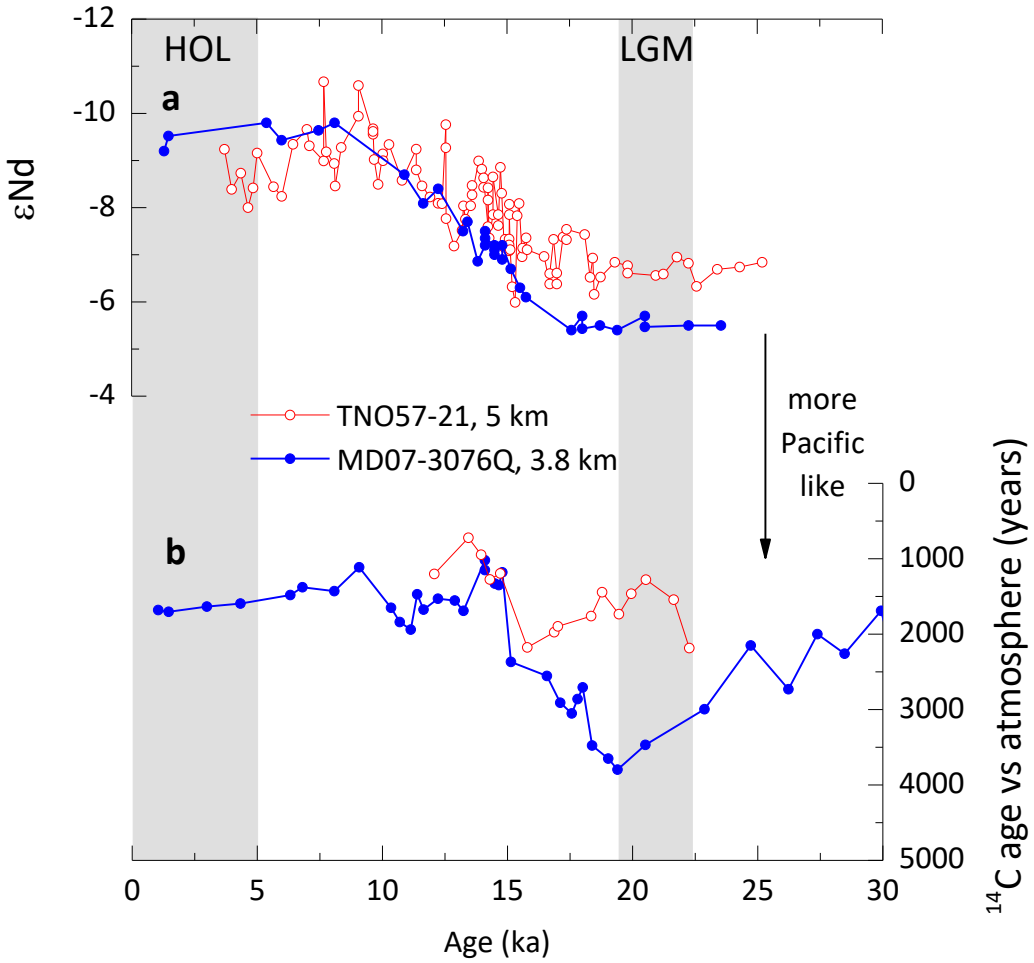

542

543

544 **Fig. 1 | Comparison of εNd and ^{14}C ages at 3.8 and 5 km water depths in the South Atlantic**
545 **Ocean. a**, εNd. **b**, ^{14}C ages. Note that the shallower core MD07-3076Q had more Pacific-like εNd
546 and ^{14}C-age signatures than the abyssal core TNO57-21 during the LGM. See Fig. 2 for core
547 locations. Data are from refs [5,6,14,15].

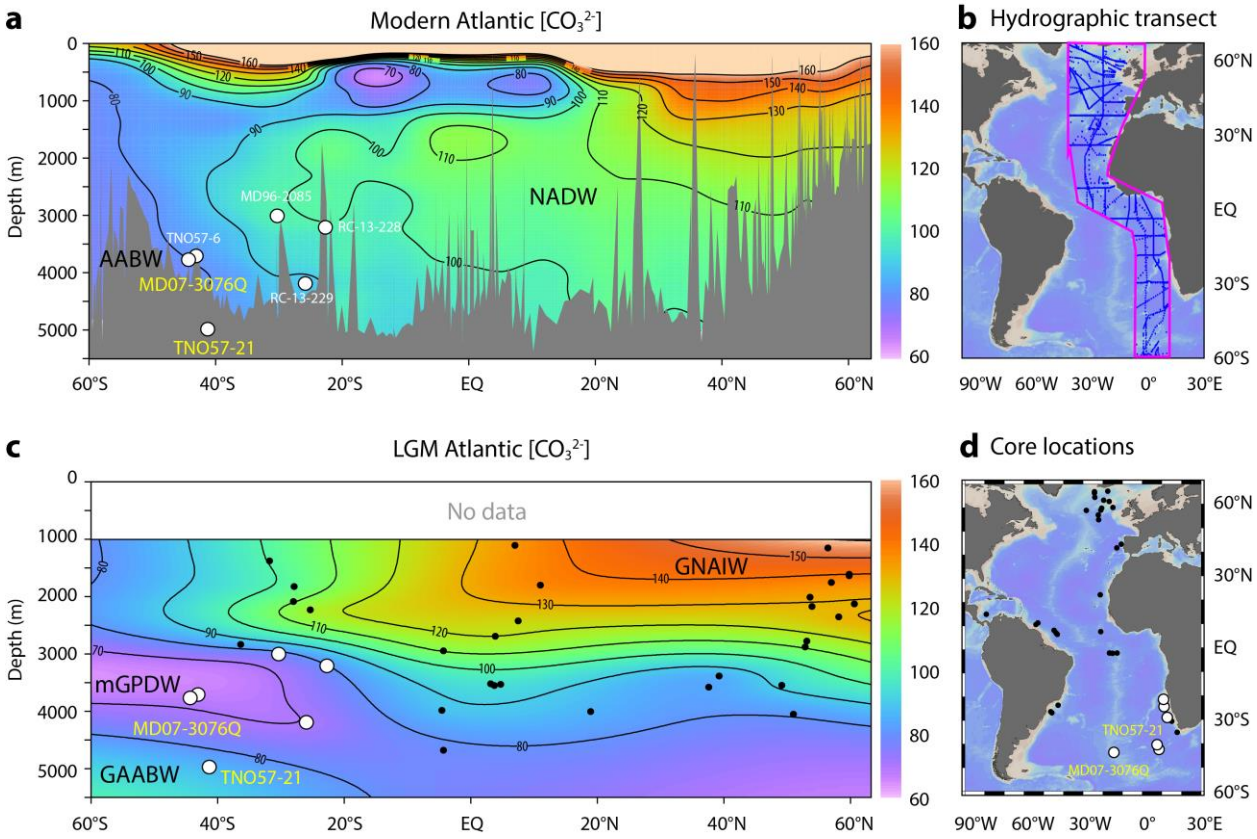

548

549

550

551 **Fig. 2 | Modern and LGM Atlantic meridional [CO_3^{2-}] transects. a**, Modern [CO_3^{2-}] transect
552 for hydrographic sites shown in **b** compiled by the GLODAP dataset[11]. **c**, Reconstructed LGM
553 [CO_3^{2-}] transect, using [CO_3^{2-}] reconstructions for all studied cores (dots and white filled circles
554 shown in **c** and **d**). White filled circles shown in **a** and **c** denote locations of the five cores at 3-4
555 km and an abyssal core at ~5 km from the South Atlantic. Bright yellow labelling indicates
556 locations of cores TNO57-21 and MD07-3076Q, whose long records are investigated (Fig. 4).
557 NADW = North Atlantic Deep Water, AABW = Antarctic Bottom Water, GNAIW = Glacial North
558 Atlantic Intermediate Water, GAABW = Glacial AABW, mGPDW = modified Glacial Pacific
559 Deep Water. Maps are generated using Ocean Data View[50] (see Methods).

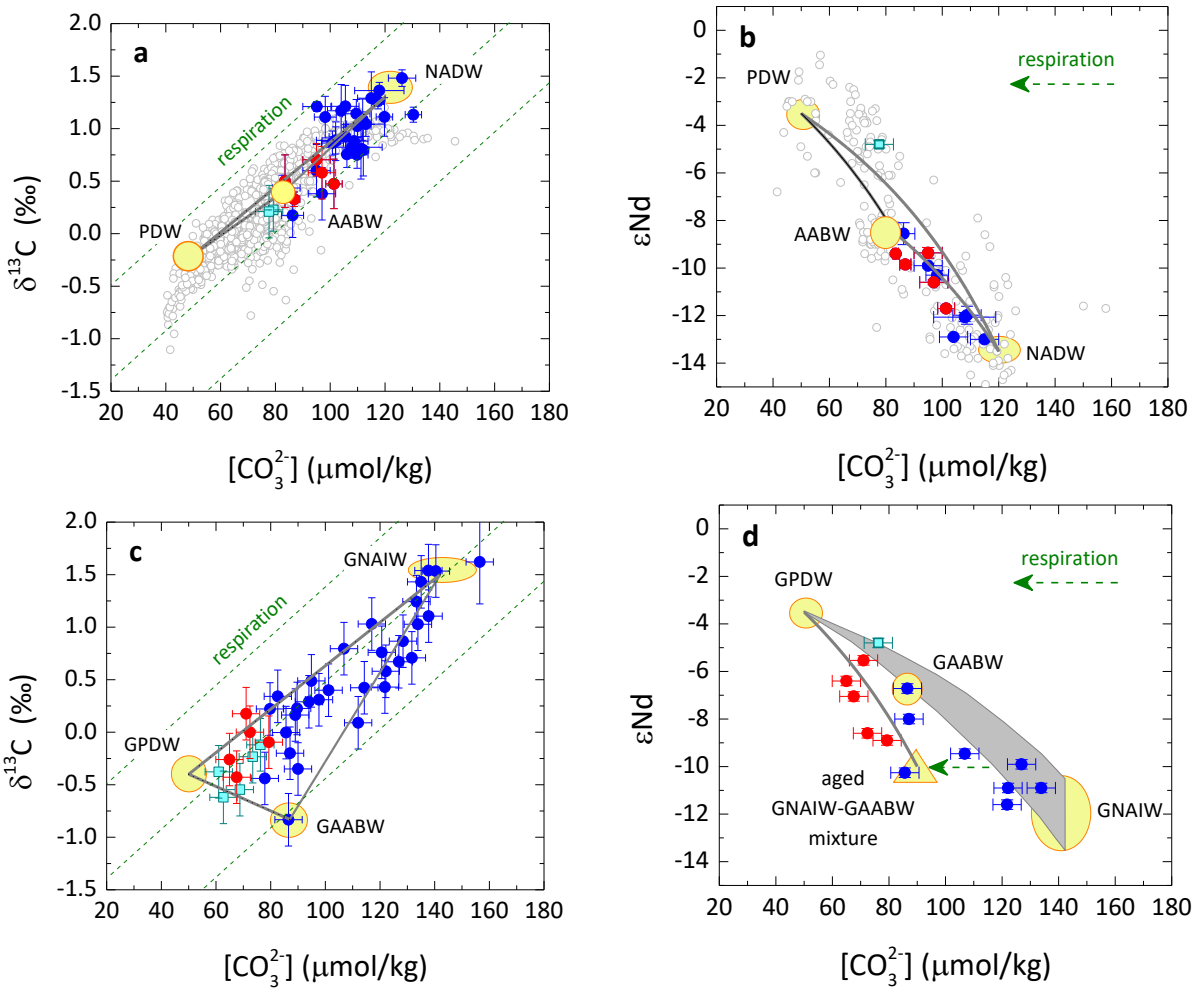

560

561

562 **Fig. 3 | Paired $[CO_3^{2-}]$-$\delta^{13}C$-εNd. a**, Holocene $\delta^{13}C$-$[CO_3^{2-}]$. **b**, Holocene εNd-$[CO_3^{2-}]$. **c**, LGM
563 $\delta^{13}C$-$[CO_3^{2-}]$. **d**, LGM εNd-$[CO_3^{2-}]$. Red circles show sites at 3-4 km from the South Atlantic (Fig.
564 2), compared with other Atlantic locations (blue circles) and sites at 3-4 km from the equatorial
565 Pacific Ocean (cyan squares). Grey circles show modern hydrographic data[11] (Supplementary
566 Table 9). Large yellow circles/ovals represent endmember values (Supplementary Table 3). The
567 yellow triangle in **d** denotes a hypothetical aged GNAIW-GAABW mixture, but also note other
568 scenarios (Supplementary Fig. 5). Green dashed lines (**a**, **c**) represent the Redfield slope[26] and
569 dashed arrows (**b**, **d**) indicate respiration effects. Grey lines/curves/shaded regions show
570 conservative mixing of water masses (Methods). The mixing curvature for $\delta^{13}C$-$[CO_3^{2-}]$ is almost
571 linear, but that for εNd-$[CO_3^{2-}]$ is much greater due to large endmember [Nd] contrasts (Methods).
572 Due to biological respiration and uncertainties associated with endmember values including [Nd]
573 and εNd (Supplementary Fig. 5-6; Methods), mixing trends should be treated as a guide for
574 qualitative, not quantitative, estimates of mixing effects.

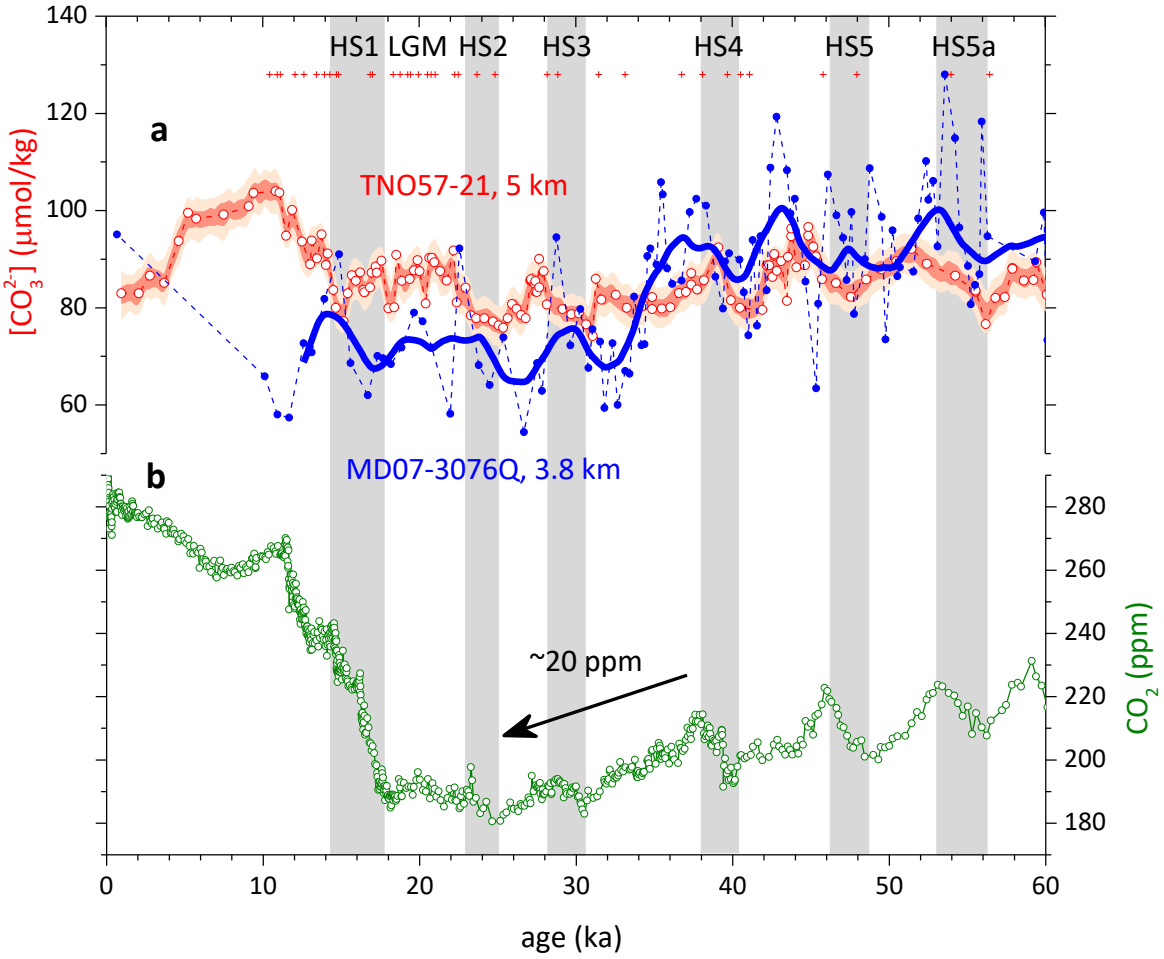

575

576 **Fig. 4 | South Atlantic [CO_3^{2-}] reconstructions at 3.8 and 5 km water depths compared with**
577 **atmospheric CO_2 during the last 60 ka**. **a**, Deep-water [CO_3^{2-}] for TNO57-21 (0-27 ka: ref. [42];
578 27-60 ka: this study) and MD07-3076Q[25]. Age models (crosses) are from ref. [24]. Dark and light
579 red envelopes represent 1σ and 2σ uncertainties, respectively (Methods). Bold blue curve shows
580 3-kyr smoothing mean. **b**, Atmospheric CO_2[45]. The arrow represents the last ~20 ppm atmospheric
581 CO_2 drawdown during the last glacial cycle which was coeval with the reversal of [CO_3^{2-}] gradient
582 between MD07-3076Q and TNO57-21. HS = Heinrich Stadial.